Self-consistent calculation of ionized-donor distribution in a nanostructured heterojunction with corrugated gate

Karlheinz Lier
Physikalisches Institut, Universität Würzburg, D-97074 Würzburg, Federal Republic of Germany

Rolf R. Gerhardts
Max-Planck-Institut für Festkörperforschung, Heisenbergstrasse 1, D-70569 Stuttgart, Federal Republic of Germany
(Received 17 May 1993; revised manuscript received 30 July 1993)

We calculate self-consistently the spatial distribution of ionized silicon donors in the barrier of a nanostructured GaAs-$Al_xGa_{1-x}As$ heterostructure with a corrugated top gate, as well as the electron density of the corresponding modulated two-dimensional electron gas (2DEG). The geometry of the periodically corrugated Schottky gate gives rise to an inhomogeneous occupation of deep donor levels (DX centers) at room temperature, which freezes in when the device is cooled down. This charge pattern can nearly compensate the desired field effect near the GaAs-$Al_xGa_{1-x}As$ interface. On the other hand, moderate doping of the barrier is predicted to lead to an improvement of the confinement potential, which affects the electrons in the 2DEG. Our numerical treatment of the laterally modulated electron density combines a Fang-Howard variational approach describing quantum confinement in the growth direction and a Thomas-Fermi approximation modeling the lateral inhomogeneities, and covers the gate-voltage-induced crossover from a weakly modulated 2DEG to isolated quantum dots.

I. INTRODUCTION

In recent years, the preparation and investigation of low-dimensional electron systems in $Al_xGa_{1-x}As$-GaAs heterostructures have attracted continuously increasing interest. Various techniques of surface preparation have been developed, in order to impose lateral constrictions on the two-dimensional electron gas (2DEG) located in the GaAs near its interface with the Si-doped $Al_xGa_{1-x}As$ barrier. A lateral density modulation of the 2DEG and, eventually, a complete depletion of electrons from certain regions of the 2DEG can be achieved either by appropriate etching techniques or by means of a laterally structured metallic gate evaporated on the sample.[1] Although these methods of nanostructuring work very successfully, it is not well known what happens inside the sample when, at room temperature, the top of the sample is etched and eventually covered by a metallic layer. In all cases, inhomogeneously distributed charges are created near the surface, which interact electrostatically with the 2DEG. However, the amount and the location of these charges and, as a consequence, the external confinement potential, which restricts the motion of electrons in the 2DEG, are not well known. This is obvious for single quantum dots, which can be defined somewhere underneath or between macroscopic gate fingers and have been investigated by magnetotunneling spectroscopy.[2,3] But it is also true for the extremely regular and over many unit cells apparently perfectly periodic structures, which have been investigated by far-infrared (FIR) spectroscopy[4–7] and by magnetotransport experiments.[8] We will demonstrate this below within a rather realistic model of a heterostructure with a strictly periodic lateral superlattice defined by a corrugated top gate. For realistic model parameters, the mere presence of the periodically corrugated gate leads to a nontrivial spatial distribution of ionized Si atoms in the $Al_xGa_{1-x}As$ barrier, which could not have been anticipated without a self-consistent numerical calculation of charge distribution and electrostatic potential in the sample.

The motivation of the present work is the fact that many experimental results, notably on FIR magnetospectroscopy of arrays of quantum dots,[7] cannot be satisfactorily understood without a good knowledge of the confinement potential defining the dot. The gross features of the FIR spectra can be explained if the confinement potential for an individual quantum dot is assumed to be parabolic. Then a generalized Kohn theorem[9] (GKT) predicts that, in the presence of a perpendicular magnetic field, the collective FIR spectrum of the dot is identical with that of a single electron moving in this parabolic potential. The characteristic fine structure of the experimentally observed FIR spectra has been explained in terms of the lowest-order deviations of the true confinement potential from its harmonic approximation.[10] In order to decide whether this explanation is correct or off the truth by orders of magnitude, one needs to know the confinement potential.

The role played by the confinement potential is the basic physical difference between an artificial atom, consisting of a quantum dot with a few electrons, and a natural atom. In the latter, the electrons are bound by the well-known Coulomb potential of the nucleus in the center of the atom. The confinement potential of an artificial atom, however, has its sources in remote charges and is not well known. The excitation spectra of natural atoms are characteristic for the elements, i.e., the num-

ber of electrons in the atom. Those of the artificial atoms depend on the electron number only because the confinement potential is not strictly parabolic. To understand the fine structure of these spectra, a good knowledge of the confinement potential is inevitable. This situation is obviously very different from that met in the magneto-transport spectroscopy of single quantum dots.[2,3] There, the characteristic features of the conductance oscillations have been observed on many different quantum dots, and thus cannot depend on details of the confining potential, which would be different for each dot.

In view of existing experiments[4–7] and possible future extensions of recent model calculations[10–12] on quantum dots with only a few electrons, it is of considerable interest to calculate the confinement potential of a periodic array of quantum dots within a realistic model. The experiments are done on arrays with typically 10^8 unit cells, so that rare imperfections, e.g., due to impurities, will not be important, and will not be considered in our model. As in experiment,[7] we will consider a GaAs-$Al_xGa_{1-x}As$ heterostructure with a corrugated metal gate. Applying a suitable gate voltage V_g, one depletes electrons locally from the 2DEG, thus increasing the density modulation while decreasing the average density of the 2DEG. This feature makes the GaAs-$Al_xGa_{1-x}As$ heterostructures very suitable for investigation of dot systems with few electrons, and distinguishes them from the metal-insulator-transistor concept recently suggested by Drexler *et al.* in order to keep the 2DEG closer to the field effect electrode.[13]

In our conventional heterostructure geometry, the relation between the periodically modulated potential created at the gate and the resulting density modulation of the 2DEG is dominated by two effects. The first is that, according to Poisson's equation, a periodic potential modulation in the xy plane, which is created at the gate, will decay exponentially in the growth (z) direction of the heterostructure. As a consequence, the modulation amplitude in a parallel plane near the 2DEG may be smaller than the modulation amplitude near the gate by several orders of magnitude. The second important effect is screening by mobile charges. At low temperatures, only screening by the 2DEG is relevant, which is linear for sufficiently small modulation amplitudes. If the potential modulation becomes too large, or equivalently, the average density of the 2DEG becomes too small, linear screening breaks down and the 2DEG may fall abruptly into disconnected pieces.[14] For an electron gas in a randomly fluctuating potential, created, for example, by statistically distributed donor charges in the $Al_xGa_{1-x}As$ barrier, this may lead to an insulating state where the electrons are localized in disconnected paddles of irregular shape.[15] If we impose a strong modulation with square symmetry, we should expect that this abrupt change of the screening behavior will favor the formation of isolated quantum dots.

At sufficiently high temperatures ($T > T_d \approx 150$ K), an additional screening effect in the Si-doped part of the $Al_xGa_{1-x}As$ barrier becomes important. Due to thermal fluctuations, deep donor levels can be populated and depopulated, and an equilibrium occupation according to the local value of the electrostatic potential will be established.[16,17] If the sample is cooled down below T_d these thermal fluctuations are suppressed, i.e., relaxation times become longer than days,[16] and the occupation of the deep donor levels is frozen in and can no longer follow the local electrostatic potential. The fact that, at low temperatures, electrons cannot recombine into ionized deep donor levels in Si-doped $Al_xGa_{1-x}As$ is known as the persistent photoconductivity effect. It was extensively exploited by the holographic nanostructuring technique used by Weiss and co-workers to produce the high-mobility samples which showed novel modulation-induced magnetoresistance oscillations.[8] The principle of this holographic technique is to ionize, at low temperature, deep donor levels with a suitable interference pattern of laser light, so that a spatially modulated, periodic arrangement of donor charges results, which defines a lateral superlattice.

If a nanostructured heterostructure, at room temperature, is covered by a corrugated Schottky gate, the occupation of deep donor levels will rearrange according to the local value of the imposed spatially modulated electrostatic potential which, in turn, is determined by the spatial distribution of charges in the doped barrier and the 2DEG and by the electrostatic boundary conditions. We will include all these effects in our self-consistent calculation, and we will see that, for realistic model parameters, spatial variation of the ionized-donor charge density is a drastic effect. Our model will be specified in detail in Sec. II A. In contrast to a previous work by Kumar, Laux, and Stern[18] calculating the ground state of a single quantum dot with a few electrons within the Hartree approximation, we consider a periodic array of quantum dots, which simplifies the electrostatic boundary conditions and facilitates comparison with experiments. Apart from some other, more technical differences, we use a Thomas-Fermi treatment of the 2DEG, which allows us to cover the whole range from a weakly modulated 2DEG to isolated dots. Furthermore, we emphasize the spatial variation of the ionized-donor density, which has not been discussed in Ref. 18. Our results for the ionized-donor distribution will be presented in Sec. III A, and the corresponding results for the dot confinement potential, which compare very favorably with experimental results, will be discussed in Sec. III B.

II. MODEL

A. Basic device parameter

The basic device parameters required for numerical calculation are fitted to the samples used in the experiments of Meurer and co-workers.[7,19] In detail, we assume a plane back gate formed by a Si δ-doping layer on top of a substrate at $z > L_3$, followed by a 330 nm undoped GaAs region in $L_s < z < L_3$. The δ layer is modeled as a surface of constant electrostatic potential at $z = L_3$ like a metallic layer but with a small effective Schottky barrier, because the Fermi level is pinned close to the conduction band by impurity states. On top of the GaAs layer

there is a 36.3 nm spacer of undoped $Al_{0.32}Ga_{0.68}As$ in $L_2 < z < L_s$ and a 56.1 nm $Al_{0.32}Ga_{0.68}As$ Si-doped layer from L_1 to L_2 (see Fig. 1). A periodic pattern is etched 100 nm deep into a subsequent 108.8 nm GaAs cap layer at $z < L_1$, which is finally covered by a metallic gate. The inset of Fig. 2 shows one unit square of the periodic corrugation shape. The input data we used for the gate corrugation $g(\mathbf{r})$ for one unit cell are created by means of a simple product of Fermi functions,

$$g(\mathbf{r}) = \frac{-d_g}{\left[1+\exp\left(\frac{|x|-a/4}{b}\right)\right]\left[1+\exp\left(\frac{|y|-a/4}{b}\right)\right]}, \quad (1)$$

where $d_g = 100$ nm denotes the etching depth, $a = 400$ nm is the lateral period, and b is chosen to be $a/25$. For the sake of clarity residues of photoresist, often integrated in optically defined lateral structures, are not taken into account. We take the conduction band offset as 410 meV. For the height of the Schottky barrier between cap layer and top gate 700 meV is assumed. An effective Schottky barrier of 50 meV is attached to the back gate describing the pinning of the Fermi level mentioned above. The binding energy of the deep and the shallow donors is taken to be 150 meV and 0 meV, respectively.[16] Following the paper of Schubert, Knecht, and Ploog[16] the portion of deep donors to the total number of impurity states depending on the Al mole fraction is 90% in our case, and the critical temperature T_d where thermal activation of occupied deep donors becomes impossible is 150 K. For the parameters used throughout this paper the shallow donors are completely ionized. Figure 2 shows the conduction band edge in growth direction for two points in the xy plane. Occupied and unoccupied impurity states are also indicated.

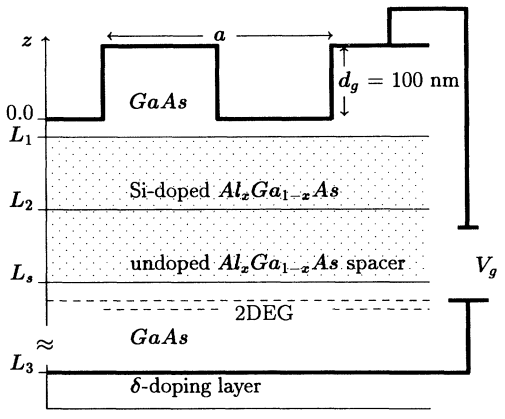

FIG. 1. Spatial arrangement of material layers and etching pattern of the model sample of our paper. The gate voltage is applied between the δ-doping layer and the nanostructured gate which are both indicated by thick lines. The modulated two-dimensional electron gas (2DEG) is sketched by dashed lines ($L_1 = 8.8$ nm, $L_2 = 64.9$ nm, $L_s = 101.2$ nm, and $L_3 = 431.2$ nm).

B. Formulation of the boundary value problem

The spatial variation of the electrostatic potential, which we describe by the potential energy $\Phi(\mathbf{x})$ of an electron of charge $-e$, between the flat and the corrugated metal gate is determined by Poisson's equation

$$\Delta\Phi(\mathbf{x}) = \rho(\mathbf{x}), \quad (2)$$

and the corresponding boundary conditions.

$$\Phi(\mathbf{r}, g(\mathbf{r})) - V_1 = 0, \qquad (\mathbf{r}, z) \equiv \mathbf{x}, \quad (3)$$

$$\Phi(\mathbf{r}, L_3) - V_2 = 0. \quad (4)$$

$\rho(\mathbf{x})$ is the charge density times $e/\epsilon_0\chi$, while ϵ_0 and χ are the dielectric susceptibility of the vacuum and the relative dielectric constant of GaAs, respectively. Considering periodicity and quadratic symmetry in the xy plane, the corrugation $g(\mathbf{r})$, the potential $\Phi(\mathbf{x})$, and the charge density $\rho(\mathbf{x})$ can be expanded in Fourier series:

$$\rho(\mathbf{x}) = \sum_{\mathbf{k}} \rho(\mathbf{k}, z)\exp(i\mathbf{k}\cdot\mathbf{r}), \quad (5)$$

$$g(\mathbf{r}) = \sum_{\mathbf{k}} g(\mathbf{k})\exp(i\mathbf{k}\cdot\mathbf{r}), \quad (6)$$

$$\Phi(\mathbf{x}) = \sum_{\mathbf{k}} \Phi(\mathbf{k}, z)\exp(i\mathbf{k}\cdot\mathbf{r}), \quad (7)$$

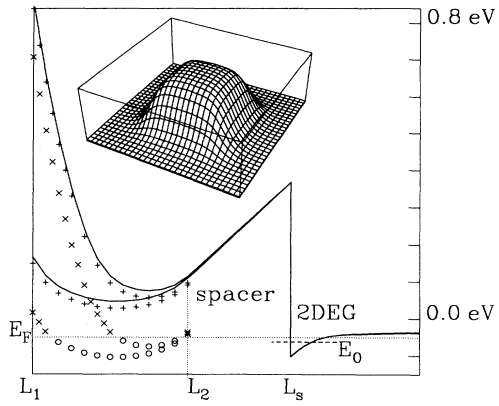

FIG. 2. Typical conduction band energy along growth direction taken at two different points in the xy plane, where the lateral potential landscape has its extrema. In the doping layer shallow donors are totally ionized and their energy levels are marked by + signs, while occupied and unoccupied deep donor states are distinguished by ○ and ×, respectively. No bias voltage ($V_g = 0$ V) is assumed and the binding energy E_0 (dashed line) is below the Fermi level E_F (horizontal dotted line), which is defined by a back gate outside the range of this figure. A weakly modulated 2DEG is established at the interface. The inset shows one unit square of the corrugation of the metal surface which acts as field effect electrode at the top of the device. In the main figure, the upper line indicates the variation of the conduction band edge below a corner of this unit square and the lower line that below the center. Here we have chosen the dopant density to be $N_0 = 1.0 \times 10^{18}$ cm^{-3} and the temperature of the equilibrium state to be 150 K.

where $\mathbf{k} = (2\pi/a)(n,m)$. Inserting Eqs. (7) and (5) in Eq. (2) we obtain the following differential equation for the amplitudes $\Phi(\mathbf{k},z)$:

$$\frac{d^2}{dz^2}\Phi(\mathbf{k},z) - |\mathbf{k}|^2\Phi(\mathbf{k},z) = \rho(\mathbf{k},z)\,. \tag{8}$$

Introducing the definition

$$R(\mathbf{k},z) = \int_{L_1}^{z} dz' \exp(-2kz') \times \int_{L_1}^{z'} dz'' \exp(kz'')\rho(\mathbf{k},z'')\,, \tag{9}$$

Eq. (8) is formally solved by the expressions

$$\Phi(\mathbf{k},z) = \Phi(\mathbf{k})\{\exp(-kz) - \exp[-k(2L_3 - z)]\} + [R(\mathbf{k},z) - R(\mathbf{k},L_3)]\exp(kz) \tag{10}$$

for $k \equiv |\mathbf{k}| \neq 0$, and

$$\Phi(\mathbf{k}=\mathbf{0},z) = \Phi(\mathbf{k}=\mathbf{0})\big[z - L_3\big] + V_2 + R(\mathbf{k}=\mathbf{0},z) - R(\mathbf{k}=\mathbf{0},L_3)\,. \tag{11}$$

One can check that the boundary condition (4) is satisfied. It remains to satisfy the boundary condition (3) as well. Since we can take only a finite set of Fourier coefficients ($\mathbf{k} \in \mathcal{K}$) into account, this can be done only approximately. We will satisfy condition (3) approximately by minimizing the boundary value mismatch defined by

$$F[\Phi^M] = \int_C d^2r |\Phi^M(\mathbf{r}, g(\mathbf{r})) - V_1|^2\,. \tag{12}$$

The integral is taken over one unit cell. The index M indicates the difference between our approximation $\Phi^M(\mathbf{x})$, taking M Fourier coefficients per lateral degree of freedom into account, and the exact potential $\Phi(\mathbf{x})$ which contains an infinite number of coefficients. At the minimum of $F[\Phi^M]$ the variation with respect to the coefficients must be zero,

$$\frac{\delta F}{\delta \Phi^M(\mathbf{k})^*} = 0\,. \tag{13}$$

We carry out the derivative explicitly, making use of Eqs. (9)–(12) and of $R(\mathbf{k}, g(\mathbf{r})) \equiv 0$, which follows from the fact that the doping layer is confined to $L_1 < z < L_2$, so that $\rho(\mathbf{x}) = 0$ for $z < L_1$. The result is

$$\sum_{\mathbf{k}'\in\mathcal{K}} \Gamma_{\mathbf{k},\mathbf{k}'}\Phi^M(\mathbf{k}') = \sum_{\mathbf{k}'\in\mathcal{K}} \Lambda_{\mathbf{k},\mathbf{k}'}\left[R(\mathbf{k}',L_3) + (V_1 - V_2)\,\delta_{\mathbf{k}',\mathbf{0}}\right]\,, \tag{14}$$

where

$$\Gamma_{\mathbf{k},\mathbf{k}'} = \int_C d^2r f(k', g(\mathbf{r}))f^*(k, g(\mathbf{r}))\exp[i(\mathbf{k}' - \mathbf{k})\mathbf{r}]\,, \tag{15}$$

$$\Lambda_{\mathbf{k},\mathbf{k}'} = \int_C d^2r \exp\left(k'g(\mathbf{r})\right)f^*(k, g(\mathbf{r}))\exp[i(\mathbf{k}' - \mathbf{k})\mathbf{r}]\,, \tag{16}$$

and

$$f(k \neq 0, z) = \exp(-kz) - \exp(-2kL_3 + kz)\,,$$
$$f(k = 0, z) = z - L_3\,.$$

We write Eq. (14) more symbolically as

$$\hat{\Gamma}\cdot\mathbf{\Phi}^M - \hat{\Lambda}\cdot\mathbf{R} = 0\,. \tag{17}$$

Equation (17) can be solved provided the matrices $\hat{\Gamma}$ and $\hat{\Lambda}$ are known. The integrals (15) and (16) defining the elements of $\hat{\Gamma}$ and $\hat{\Lambda}$ are determined by the function $g(\mathbf{r})$ describing the corrugation of the gate, and must be calculated numerically. We have inverted the matrix $\hat{\Gamma}$ and then multiplied by $\hat{\Lambda}$. The resulting matrix $\hat{\Omega} = \hat{\Gamma}^{-1}\cdot\hat{\Lambda}$ applied to the vector $\mathbf{R}$ which includes complete information about inhomogeneities gives the best approximation of the Fourier coefficients represented by the components of the vector $\mathbf{\Phi}^M$. This is one essential part of the self-consistency loop. A given charge distribution is transformed into the related electrostatic potential with the correct boundary conditions up to an error only due to limitation to a finite set of Fourier coefficients.

For practical purpose M=8 Fourier components for each lateral degree of freedom are sufficient to obtain a relative error δ in the potential amplitudes less than 1%, where we have defined δ by

$$\delta = \sum_{\mathbf{k}\in\mathcal{K}} |\Phi^M(\mathbf{k}) - \Phi^{12}(\mathbf{k})| \Big/ \sum_{\mathbf{k}\in\mathcal{K}} |\Phi^{12}(\mathbf{k})|\,,$$

taking the calculation with M=12 as a reference. Going beyond M=16 we achieved no improvement of the accuracy due to rounding errors. Note that δ gives no direct information about how well the boundary condition (3) is fulfilled. Also $F[\Phi^M]$ itself is not an appropriate measure for checking (3), because $F[\Phi^M]$ must in principle be zero. Therefore we considered $Q = F[\Phi^M]\,/\,F[\Phi^0]$, which reflects the improvement of $F[\Phi^M]$ going from zero to M Fourier components. For our model calculation we checked that Q was about 0.1%. Since $F[\Phi^0]$ is a measure for the potential variation between the bottom and the top of the gate in the absence of lateral potential modulations, Q measures the effectiveness of the M Fourier components in reducing the mismatch $F[\Phi^0]$ all over the surface $z = g(\mathbf{r})$.

Before going into further details of the self-consistent calculations some general properties of our model should be noticed. In the following we neglect in the notation the subtle difference between exact and numerical values, i.e., omit the superscript M.

First, for a flat gate, i.e., $g(\mathbf{r})$=const, one sees immediately that the matrices defined in (16) and (15) are diagonal and thus $\hat{\Omega}$ is diagonal, too. According to the fact that $V_1 - V_2$ differs from the gate voltage V_g only by a constant ΔE_s caused by different Schottky barriers,

we can conclude with (14), that in the presence of a flat gate, only the lateral mean value of the electrostatic potential, i.e., $\Phi(\mathbf{k}=\mathbf{0},z)$, can be manipulated by applying a gate voltage. In other words, any potential fluctuations remain unaffected by a flat gate geometry.

Second, let us consider the case of a corrugated gate. Then the off-diagonal elements of $\hat{\Omega}$ do not vanish and Eq. (14) yields a linear relation between the potential amplitudes $\Phi(\mathbf{k})$ and the gate voltage V_g,

$$\Phi(\mathbf{k}) = \Omega_{\mathbf{k},\mathbf{0}}\left[\Delta E_s + V_g\right] + \sum_{\mathbf{k}'} \Omega_{\mathbf{k},\mathbf{k}'} R(\mathbf{k}', L_3)\,. \quad (18)$$

It follows that, for a laterally homogeneous charge density, i.e., if $R(\mathbf{k}, L_3) = 0$ for $\mathbf{k} \neq 0$, the electrostatic potential is also laterally homogeneous for a certain value of the gate voltage V_g^0,

$$V_g^0 = -\Delta E_s - R(\mathbf{0}, L_3)\,, \quad (19)$$

which is independent of the corrugation $g(\mathbf{r})$.

The linear dependence Eq. (18) of $\Phi(\mathbf{k})$, and, as a consequence, of the confinement potential of an array of quantum dots, on the gate voltage V_g may resolve an apparent discrepancy between the statement of the generalized Kohn theorem and experimental findings.[20] If, with a sufficient accuracy, the confinement potential of an individual quantum dot can be assumed to be parabolic,

$$V(x,y) = \tfrac{1}{2} m^* \omega_0^2 \left[x^2 + y^2\right], \quad (20)$$

one expects from the GKT to see in the FIR response at zero magnetic field a resonance at the frequency ω_0. This result should be independent of the number of electrons in the dot and of Coulomb interaction effects. The observed linear dependence of the square of the resonance frequency on the gate voltage[20] seems on the other hand to indicate a dependence on the electron number, which, according to the common capacitor rule, is expected to increase linearly with the gate voltage. However, if one defines the confinement frequency ω_0 according to

$$\omega_0^2 = \frac{1}{m^*}\frac{\partial^2 V(x,0)}{\partial x^2} = \frac{1}{m^*}\frac{\partial^2 V(0,y)}{\partial y^2} \quad (21)$$

and calculates $V(x,y)$ from $\Phi(\mathbf{x})$ as defined by Eqs. (7)–(11), one obtains from Eq. (18) a linear dependence of ω_0^2 on the gate voltage V_g, as observed in experiment, and without any contradiction against the GKT.

C. Model of charge distribution

If one knows the charge distribution $\rho(\mathbf{x})$ inside the sample, the formalism of Sec. II B gives the corresponding potential with the correct boundary values.

In an explicit way one can obtain the ionization profile in the doping layer by occupying, according to Fermi statistics, the donor levels which are assumed as homogeneously distributed between L_1 and L_2:

$$\begin{aligned}\rho_d(\mathbf{x}) = {} & eN_0[\Theta(z-L_1) - \Theta(z-L_2)] \\ & \times\{1 - \xi f([\Phi(\mathbf{x}) + E_c - E_{sd} - \mu]/k_BT) \\ & -(1-\xi) f([\Phi(\mathbf{x}) + E_c - E_{dd} - \mu]/k_BT)\}\,, \quad (22)\end{aligned}$$

where N_0 denotes the impurity concentration, E_c the conduction band offset, and E_{dd} and E_{sd} the binding energy of deep and shallow donors, respectively. $f(x)$ is the Fermi function and ξ the fraction of shallow donors to the total impurity concentration.

We assume the Si-dopant density in the layer $L_1 < z < L_2$ to be homogeneous, since fluctuations on a length scale of the mean distance between impurities ($\sim 10\,\mathrm{nm}$ for $N_0 \sim 10^{18}\,\mathrm{cm}^{-3}$) according to Poisson's equation will not affect the 2DEG. Also fluctuations on a scale much larger than the period a of our lateral superlattice will be effectively screened by the mobile donator charges at high temperatures. Random fluctuations of the dopant density on a length scale comparable with the period a might disturb our results and lead, e.g., to fluctuations of the confinement potential for isolated quantum dots. There is no experimental evidence that such fluctuations should be relevant[7,19] and we neglect such complications.

Since our aim is to calculate the distribution $\rho_d(\mathbf{x})$ of ionized donors, we restrict ourselves to a rather crude model for the 2DEG. Assuming that the lateral variation of the electron density happens on a much larger scale than the variation in z direction, we employ an adiabatic, Born-Oppenheimer-type approximation for the electronic charge density,

$$\rho_{\mathrm{FH}}(\beta, \mathbf{x}) = -e n_s(\mathbf{r})\,|\varphi_{\mathrm{FH}}(\beta, z)|^2\,, \quad (23)$$

and treat the lateral 2D density $n_s(\mathbf{r})$ in a quasiclassical Thomas-Fermi approximation (TFA). This should be an excellent approximation for variations of $n_s(\mathbf{r})$ on a scale much larger than the typical extent of wave functions, i.e., the Fermi wavelength or mean distance between electrons ($\lesssim 50\,\mathrm{nm}$), but not for isolated quantum dots containing only a few electrons. Indeed, the successful application of the TFA to randomly distributed electrons in a stripe by Nixon and Davies[15] and the explanation of self-consistent Hartree results for a one-dimensionally modulated 2DEG in terms of the TFA (Ref. 14) indicates that the TFA works reasonably well for equilibrium properties of submicrometer-structured semiconductor samples, even near the threshold between a strongly modulated 2DEG and isolated 1D or 0D regions containing many electrons.

The z direction is treated quantum mechanically. We assume that a single quantum state (subband) is occupied and describe it by a Fang-Howard variational ansatz with the wave function

$$\varphi_{\mathrm{FH}}(\beta, z) = \left[\frac{\beta^3}{2}\right]^{\frac{1}{2}} \left[z - L_s\right] \exp\left(\frac{-\beta(z-L_s)}{2}\right), \quad (24)$$

defined for $z > L_s$. In the spirit of the adiabatic approximation, β should depend on the lateral position $\mathbf{r}$.

For the sake of simplicity, we will, however, optimize the value of β for the position $\mathbf{r}_0$ at which $n_s(\mathbf{r})$ becomes maximum, and we will take this $\beta(\mathbf{r}_0)$ for all $\mathbf{r}$.

To optimize β we proceed as follows. First we set $\beta = b$ in Eq. (23) and determine from the total charge distribution

$$\rho(\mathbf{x}) = (e/\epsilon_0\chi)\left[\rho_d(\mathbf{x}) + \rho_{\mathrm{FH}}(b,\mathbf{x})\right]$$

the electrostatic potential $\Phi(b,\mathbf{x})$, following the procedure of Sec. II B. Next we consider the expectation value of the energy of an electron in this potential with the wave function (24),

$$E_{\mathrm{tot}}(\beta,b,\mathbf{r}_0) = \left\langle \varphi_{\mathrm{FH}}(\beta)\left| -\frac{\hbar^2}{2m^*}\frac{d^2}{dz^2} + \Phi(b,z,\mathbf{r}_0)\right|\varphi_{\mathrm{FH}}(\beta)\right\rangle . \tag{25}$$

Note that all the z integrations necessary for the evaluation of $\Phi(b,\mathbf{x})$ and $E_{\mathrm{tot}}(\beta,b,\mathbf{r}_0)$ can be done analytically, so that the derivative with respect to β, which is necessary to minimize $E_{\mathrm{tot}}(\beta,b,\mathbf{r}_0)$, can also be taken analytically. To obtain self-consistency of wave function and potential, we have to evaluate the extremal condition for $\beta = b$,

$$\left[\frac{\partial}{\partial\beta}E_{\mathrm{tot}}(\beta,b,\mathbf{r}_0)\right]_{\beta=b} = 0 . \tag{26}$$

This implicit equation must be solved numerically and determines b for a given input density $n_s(\mathbf{r})$ of the 2DEG.

The sheet density $n_s(\mathbf{r})$ as a function of the chemical potential defined by the back contact is modeled within the framework of the Thomas-Fermi approximation. Describing the lateral density modulation of the 2DEG by a weighted 2D density of states we write

$$n_s(\mathbf{r}) = \frac{m^* k_B T}{\pi\hbar^2}\ln\left[1+\exp\left(\frac{\mu - E_{\mathrm{tot}} - \tilde{\Phi}(b,\bar{z},\mathbf{r})}{k_B T}\right)\right] , \tag{27}$$

where the expectation value

$$\bar{z} = \langle\varphi_{\mathrm{FH}}|z|\varphi_{\mathrm{FH}}\rangle = L_s + 3/b ,$$

fixes the xy plane from which we have to read the values of the potential modulation:

$$\tilde{\Phi}(b,z,\mathbf{r}) = \Phi(b,z,\mathbf{r}) - \Phi(b,z,\mathbf{r}_0) . \tag{28}$$

In each iteration step we start with input values of $\rho_d(\mathbf{x})$ and $n_s(\mathbf{r})$ and calculate b from Eq. (26). This yields $\Phi(\mathbf{x}) = \Phi(b,\mathbf{x})$, and new values of $\rho_d(\mathbf{x})$ and $n_s(\mathbf{r})$ according to Eqs. (22) and (27). If Eqs. (22)–(28) hold simultaneously, self-consistency is achieved.

At the critical temperature ($T = T_d$) both $\rho_d(\mathbf{x})$ and $\rho_{\mathrm{FH}}(b,\mathbf{x})$ are still variable, while at lower temperatures $\rho_d(\mathbf{x})$ is assumed to be unchangeable. Thus expression (22) is in some sense only valid for ($T > T_d$). For the calculation of properties of the modulated 2DEG at low temperatures ($T < T_d$), one should take a frozen-in ionized-donor distribution $\rho_d(\mathbf{x})$ calculated at $T = T_d$.

III. RESULTS

A. Ionization profile

In the following we will present some numerical results, to illuminate the influence of inhomogeneously ionized-donor states on the electrostatic properties of the sample characterized by Fig. 2. As can be seen, the potential modulation near the region of the 2DEG is strongly suppressed as compared with that in the doping region close to the gate. The occupation probability of deep donor states, which are located near the Fermi level, is sensitive to the lateral variation of the conduction band edge. In this way a space charge pattern is created, which compensates potential modulation effectively, so that the band edge dispersion near the interface at L_s, on the scale chosen in Fig. 2, looks like that of an unstructured sample.

Figures 3 and 4 display the correspondence and mutual dependence of lateral variation of the band edge energy and space charge distribution. The data are taken along a line defined by $x = y$, and along the growth direction. The 3D presentation offers an intuitive and geometrical impression of the global physical situation.

More quantitative insight is given by Fig. 5 for which

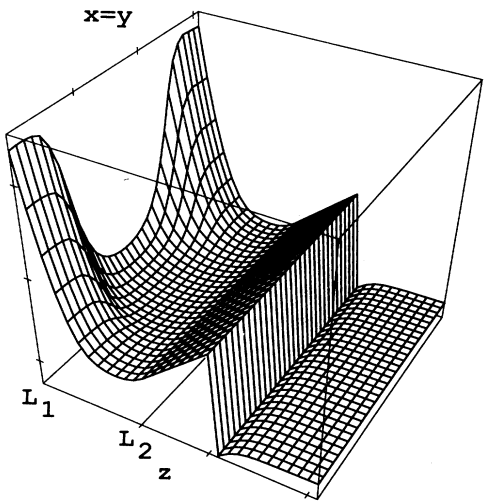

FIG. 3. Three-dimensional plot of the potential landscape for the parameters given in Fig. 2. The coordinates vary in growth direction (z) and laterally along the line $x = y$.

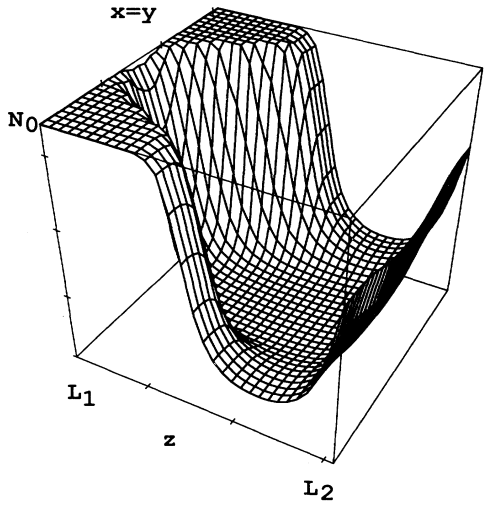

FIG. 4. Three-dimensional plot of the space charge distribution corresponding to the potential landscape of Fig. 3. The z range of the plot is limited to the region of the doping layer.

we introduce two kinds of quantities: The laterally averaged mean value $\bar{N}_d(z)$ defined as follows:

$$\bar{N}_d(z) = \frac{1}{a^2} \int_C d^2r \rho_d(\mathbf{x}) , \tag{29}$$

and the standard deviation $\sigma(z)$ defined by

$$\sigma(z)^2 = \frac{1}{a^2} \int_C d^2r [\rho_d(\mathbf{x}) - \bar{N}_d(z)]^2 . \tag{30}$$

$\bar{N}_d(z)$ measures the degree of depopulation of donor states in a plane located at z, while $\sigma(z)$ contains information about the amount of lateral variation in this plane. The plot in Fig. 5 shows these two moments of the lateral charge distribution function for three different Si-doping levels. First we notice that modulations get weaker with decreasing impurity concentration. Furthermore, a correlation between the peak value of $\sigma(z)$ and the maximum slope of $\bar{N}_d(z)$ can be seen. This is due to the fact that, on the one side, close to the gate almost every donor state is ionized, on the other side, in the right half of the doping layer there are only a few percent of the states ionized. In both situations $\sigma(z)$ is very small. It is obvious that between these limits there is a region where the lateral alternating of population and depopulation causes a high value of $\sigma(z)$. Simultaneously the spatial transition from weakly to highly ionized regions takes place and leads to a pronounced slope of $\bar{N}_d(z)$. Towards the edge of the spacer at L_2, one can observe that the degree of ionization $\bar{N}_d(z)$ increases again. This is forced by an increasing of the conduction band edge and is remarkably not accompanied by strong lateral charge fluctuations. This indicates that the corresponding lateral fluctuations of the band edge have already died out, as can also be seen in Fig. 6.

To learn more about the interplay between band bending effect and compensation of the lateral field effect we performed a numerical experiment. We repeated the self-consistent calculation (at $T = 150$ K) for three values of the applied gate voltage ($V_g = -1.0$ V, 0.0 V, and 0.5 V). The resulting $\bar{N}_d(z)$ and $\sigma(z)$ are plotted in Fig. 6. The center of the region with large lateral fluctuations $\sigma(z)$ of the occupation probability shifts with increasing negative V_g and its width gets enlarged, while the peak value remains constant. This can be understood within the picture of electric-field-induced surface charges. An

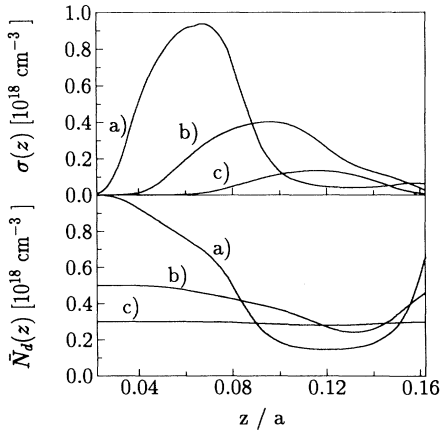

FIG. 5. The lower part of this figure shows in units of $N_0 = 10^{18}$ cm^{-3} the laterally averaged ionization profile $\bar{N}_d(z)$ for three different impurity concentrations: (a) $N_0 = 1.0 \times 10^{18}$ cm^{-3}, (b) $N_0 = 0.5 \times 10^{18}$ cm^{-3}, (c) $N_0 = 0.3 \times 10^{18}$ cm^{-3}. In the upper part the corresponding standard deviations for the three cases are plotted. The z range of the plot is identical with the extent of the doping layer, i.e., $L_1 < z < L_2$. L_s lies outside the scope of this plot. The fundamental period of our model is taken to be $a = 400$ nm throughout this paper.

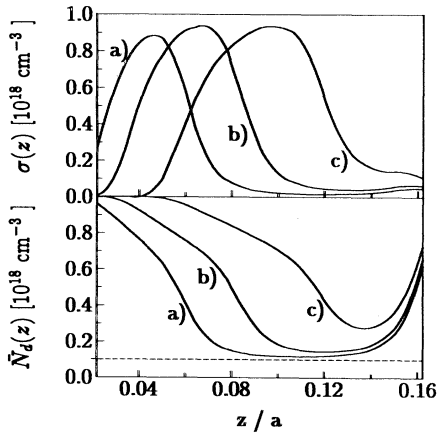

FIG. 6. The lower part of this figure shows the laterally averaged ionization profile $\bar{N}_d(z)$ for three different cool-down conditions: (a) $V_g = 0.5$ V, (b) $V_g = 0.0$ V, (c) $V_g = -1.0$ V. The impurity concentration is always 1.0×10^{18} cm^{-3}. The dashed horizontal line reflects the contribution of shallow donors to the total space charge distributions (a), (b), and (c). In the upper part the corresponding standard deviations for the three cases are plotted also. z range and the period a are the same as in Fig. 5.

increasing of the negative voltage drop relative to the back gate causes an excess of negative charges on the metal gate. These attract positive charges from the doping layer or, in other words, ionize the impurities. As a consequence the donor states will be more and more depopulated if one increases the negative bias voltage $-V_g$ until $\bar{N}_d(z)$ reaches the saturation value N_0 [see $\bar{N}_d(z)$ of Fig. 6].

Let us briefly reexamine the situation addressed in Eq. (19), where the potential modulation can be switched off by a suitable gate voltage. This situation occurs as soon as we have no electric field inside a finite layer containing the top gate. Then the potential is constant everywhere and any surface inside this region is a surface of constant potential. The boundary value problem of Sec. II then is solved trivially, i.e., the vector **R** in Eq. (17) equals zero. In a real sample, however, we have always a finite field component in the growth direction at the gate, which has its sources in different Schottky barriers and ionized impurities, so that the influence of the gate is usually not switched off even in the case of zero gate voltage. Finally, a more negative voltage results in a stronger **E** field near the gate, which enhances the lateral field effect inside the sample. At the same time the increasing compensation via lateral charge separation in the doping layer causes the enlarged width of $\sigma(z)$ in Fig. 6 [curve (c)].

B. Properties of the 2DEG

We now address the most interesting question, how the spatial distribution of ionized donors affects the properties of the 2DEG. First, we consider the situation where the 2DEG breaks up into an array of isolated quantum dots and calculate some characteristics of the confinement potential. Specifically, we calculate the confinement energy $\hbar\omega_0$, obtained according to Eqs. (20) and (21) from the parabolic approximation of the potential in the center of a quantum dot, and the lowest-order corrections to this approximation. *Ad hoc* assumptions on these quantities have previously been used to explain characteristic features of FIR resonance spectra of quantum dots.[10]

In order to eliminate any artifacts due to our simple Thomas-Fermi treatment of the 2DEG, we proceed in two steps. First, we calculate self-consistently at T_d = 150 K for three values of the gate voltage and for several values of the Si-doping level the spatial distribution of ionized donors and of electrons in the 2DEG. In this step the use of the TFA is not critical, since the ionized-donor distribution will not depend sensitively on fine details of the density variation in the 2DEG. In the second step (at low temperature T = 4 K) we freeze in the ionized-donor distribution calculated at T_d and apply now that threshold gate voltage $V_{\rm th}$ at which the depletion of the 2DEG is just complete. For this situation, where no electrons are in the dots and thus the TFA is of no relevance, we determine the characteristics of the "bare" confinement potential for electrons in the quantum dots. The threshold voltage $V_{\rm th}$ depends, of course, on the gate voltage applied at $T = T_d$ and on the Si-doping level N_0. In Fig. 7 we present for three values of V_g (our "cool-down conditions") the confinement energy $\hbar\omega_0$, calculated at the threshold $V_{\rm th}$, as a function of the Si-doping level N_0. The z value (distance from the interface between spacer and GaAs) at which the confinement potential is evaluated is indicated by the vertical dotted line in Fig. 8 and chosen near the expected center of the dots. Results for the same cool-down condition (same value of V_g) are connected by solid lines in Fig. 7. The data

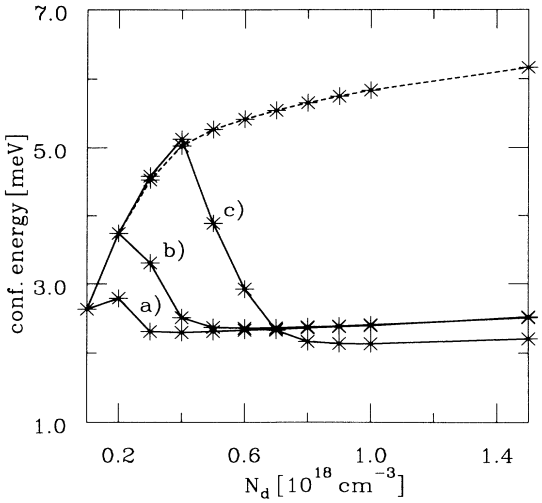

FIG. 7. Confinement energy vs impurity concentration for different cool-down conditions: (a) V_g = 0.5 V, (b) V_g = 0.0 V, (c) V_g = −1.0 V. Any star represents a complete self-consistent calculation at 150 K and a subsequent numerical determination of the confinement energy at 4 K, where a negative bias voltage is applied, so that the channel is just depleted. The solid lines connect data points with identical cool-down conditions. The dashed line is adjusted to a set of reference data one obtains by homogeneously smearing out the space charges of case (b) over the whole doping region.

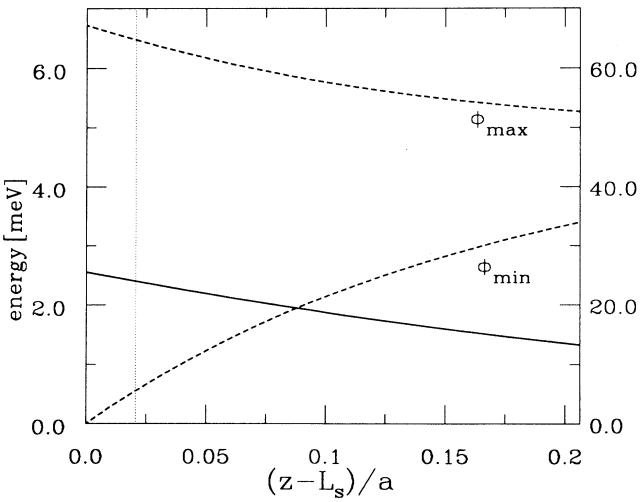

FIG. 8. The extremal values ($\Phi_{\rm min}$ and $\Phi_{\rm max}$) of the potential landscape (dashed lines, right scale) and the confinement energy $\hbar\omega_0$ (solid line, left scale) as a function of the distance from the interface.

points connected by the dashed line are obtained by a different procedure. First, at $T = T_d$, the spatial distribution $\rho_d(\mathbf{x})$ of ionized donors was calculated without applied gate voltage, $V_g = 0$, as for curve (b). Then, however, this positive charge was homogeneously redistributed over the total Si-doped volume, and with this homogeneous positive space charge (in $L_1 < z < L_2$) the confinement energy was calculated at $T = 4$ K. This procedure eliminates the screening of the gate-induced potential modulation by spatial redistribution of donor charges at elevated temperatures ($T \gtrsim T_d$). Comparison with the data sets (a)–(c) demonstrates that, for a sufficiently high doping level ($N_0 \gtrsim 0.6 \times 10^{18}$ cm^{-3}), this screening mechanism is very efficient and leads to a considerable reduction of the confinement energy, which then depends only weakly on the Si-doping level N_0 and on the cool-down condition. The resulting small $\hbar\omega_0$ values ($\sim 2-3$ meV) compare very favorably with typical experimental data.[5,7,19] We take this as a strong indication for the relevance of our model, which relies on the existence of the deep donor states and the possibility of their thermal (re)occupation at elevated temperatures ($T \gtrsim 150$ K).[16]

A completely different situation is found at low impurity densities ($N_0 < 0.6 \times 10^{18}$ cm^{-3}). As long as the Fermi level is low enough so that recombination of ionized impurity states with electrons is impossible, the positive charge in the doping layer is homogeneous. Consequently, there is no difference between the data of case (b) and the reference data (dashed line). As soon as neutralization of ionized states takes place, lateral inhomogeneities are produced and screening by ionized-donor charges becomes effective. The higher the degree of ionization, the stronger is the band bending along the growth direction. In this way deep donor states come below the Fermi level. In the case of low doping this effect can be suppressed by applying a negative voltage, as can be realized by comparison of the data sets (a) and (c). In highly doped devices the possibility of manipulation in this way is rather poor.

Further characteristics of the confinement potential are the lowest-order corrections to the parabolic approximation. With square symmetry in the xy plane, these can be expressed by the parameters a and b in the expansion[10]

$$V(x,y) = \tfrac{1}{2}m^*[\omega_0^2(x^2+y^2) + \omega_4^2 a(x^2+y^2)^2 + \omega_4^2 b(x^2y^2)]\,. \tag{31}$$

As a consequence of Eq. (14) we have already pointed out that, according to Eq. (18), the potential $\Phi(\mathbf{x})$ depends linearly on the gate voltage V_g. The same is true for spatial derivatives of $\Phi(\mathbf{x})$, so that the parameters $a(V_g)$ and $b(V_g)$ obey linear relations of the form

$$A(V_g) = A(V_{\rm th}) + [V_g - V_{\rm th}]B\,, \tag{32}$$

where $V_{\rm th}$ denotes the threshold voltage discussed before. In Table I we list the coefficients $A(V_{\rm th})$ and B for $a(V_g)$, $b(V_g)$, and other characteristics of the confinement potential. For this purpose we take ω_4^2 as $10^{-10}\omega_0^2(V_g = V_{\rm th})$ in accordance with Ref. 10. The mechanism of the resonance peak splitting suggested in Ref. 10 has its starting point in rotation-symmetry breaking and nonparabolic terms introduced by Eq. (31). Our results confirm this explanation because the deviations from the pure parabolic confinement are even stronger than estimated in Ref. 10.

TABLE I. List of data necessary to determine the model potential of (31) according to Eq. (32). In addition, threshold value and slope for the potential minimum $\Phi(\mathbf{r}_0)$ are given. The fixed xy plane is chosen near the interface at L_s as indicated in Fig. 8. The impurity concentration N_0 of the sample under consideration is taken to be 1.0×10^{18} cm^{-3} and no bias voltage is applied at elevated temperatures.

	$A(V_{\rm th} = -0.82\ \text{V})$	B
$\Phi(\mathbf{r}_0)$	-13.65 meV	-195 meV V^{-1}
$(\hbar\omega_0)^2$	6.05 meV^2	-0.46 meV^2 V^{-1}
a	-15.7×10^2 Å^{-2}	1.5×10^2 Å^{-2} V^{-1}
b	46.5×10^2 Å^{-2}	-2.1×10^2 Å^{-2} V^{-1}

Finally, we want to discuss within our simple Thomas-Fermi approximation the density distribution in the 2DEG. Although exchange and correlation effects, and even the discreteness of the electronic charge in an isolated quantum dot, are not included in our model, it is of interest to study its implications as a possible refer-

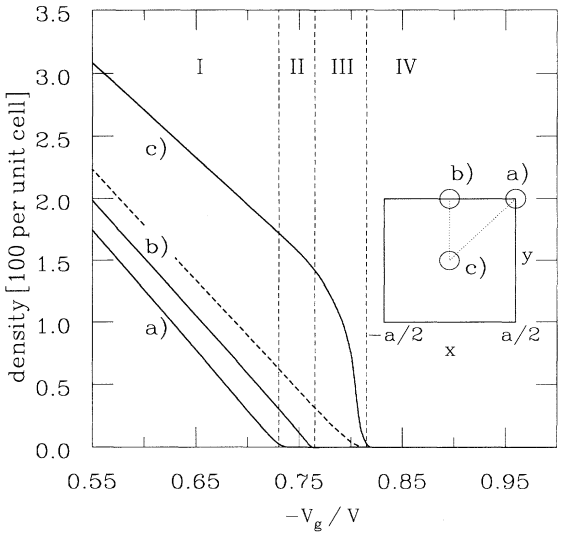

FIG. 9. Gate-voltage dependence of the sheet density as defined in Eq. (27). The density values are taken at three different points of the unit square as indicated in the right inset. Four distinct cases are covered: modulated 2DEG (I), antidots (II), dots (III), and finally the empty channel (IV) (solid lines). In the case of isolated dots the averaged sheet density per unit cell (dashed line) shows up the charge of a single dot.

ence for future more sophisticated work. Our model has the advantage that it describes the weakly modulated case and the case of isolated dots as well, which is hardly possible within a strictly quantum mechanical treatment. Exchange and correlation effects and especially the discreteness of charge will become important in the limit of only a few electrons per dot, and then our TFA will fail. In Fig. 9 we plot the electron number per unit cell to clarify where this may happen.

From physical intuition it is clear that with increasing negative gate voltage $-V_g$ the modulation of the 2DEG gets stronger and, perhaps, certain areas of local depletion arise, before a further increasing leads to the transition to isolated electron islands. For a quantitative treatment we plotted three indicating key values of the numerically calculated electron sheet density vs $-V_g$ in Fig. 9. As can be seen there, a hole in the electron sheet (antidot) occurs at the point (a) of the unit square (I $\rightarrow$ II) (see inset of Fig. 9). When the density vanishes at point (b) the last bond between different cells is broken. The zero dimensional limit is reached (III). At the threshold voltage ($V_{\rm th} = -0.82$ V) no charge can be found even at (c), i.e., the 2D channel is completely empty (IV). It is remarkable that the nearly linear gate-voltage dependence of the local density found in (I, II), no longer holds in the case of isolated dots (III), where the dimensionality of the electronic system is reduced, and a more rapid decrease leads to an abrupt depletion of the dot at $V_{\rm th}$. Moreover the existence of antidots is limited to a small gate-voltage regime ($\delta V_g = 0.4$ V), which agrees with experimentally measured values on samples with the same geometry.[19] This sensitively geometry-dependent effect can be considered as a rather significant test of the qualitative correctness of our model assumptions.

IV. CONCLUSIONS

We presented self-consistent calculations treating the inhomogeneously ionized deep donor states in nanostructured heterojunctions.

Space charge patterns inside the doping layer can compensate the lateral field effect of a structured gate to a large extent. In addition to the charge-independent exponentially dying out of every Fourier coefficient by means of Poisson's equation, the influence of such space charges should be taken into account on the way to improve the lateral field effect of submicrometer-structured gate electrodes, because they are, other than randomly distributed charges, a characteristic of design parameters. Therefore we numerically investigated the dependence of the confinement energy $\hbar\omega_0$ on the Si-doping level and on different cool-down conditions. From our results it is evident that a thin and only moderately doped layer should improve the desired confinement potential in the channel in the best way, because recombination of ionized deep donors at room temperature is so avoided. We discussed the linear gate-voltage dependence of the squared one-particle confinement energy, $(\hbar\omega_0)^2$, which can be understood as an ordinary electrostatic effect. This fact does not explain the linear dependence of the squared plasma frequency observed in FIR experiments quantitatively, but should be included in forthcoming calculations. Our data support the arguments of Ref. 10, that the mechanism of the resonance splitting is due to rotation-symmetry breaking and nonparabolic terms.

As a final point emphasizing the relevance of our model, we were able to reproduce the crossover from the modulated 2DEG to the case of isolated quantum dots within a realistic gate-voltage regime.

[1] W. Hansen, J.P. Kotthaus, and U. Merkt, in *Semimetal and Semiconductor*, edited by M. Reed (Academic Press, New York, 1992), Vol. 35, p. 279.

[2] P.L. McEuen, E.B. Foxman, U. Meirav, M.A. Kastner, Y. Meir, N.S. Wingreen, and S.J. Wind, Phys. Rev. Lett. **66**, 1926 (1991).

[3] J. Weis, R.J. Haug, K. v. Klitzing, and K. Ploog, Phys. Rev. B **46**, 12 837 (1992).

[4] Ch. Sikorski and U. Merkt, Phys. Rev. Lett. **62**, 2164 (1989).

[5] T. Demel, D. Heitmann, P. Grambow, and K. Ploog, Phys. Rev. Lett. **64**, 788 (1990).

[6] A. Lorke, J.P. Kotthaus, and K. Ploog, Phys. Rev. Lett. **64**, 2559 (1990).

[7] B. Meurer, D. Heitmann, and K. Ploog, Phys. Rev. Lett. **68**, 1371 (1992).

[8] D. Weiss, C. Zhang, R.R. Gerhardts, K. von Klitzing, and G. Weimann, Phys. Rev. B **39**, 13 020 (1989); D. Weiss, K. von Klitzing, K. Ploog, and G. Weimann, Europhys. Lett. **8**, 179 (1989); R.R. Gerhardts, D. Weiss, and K. von Klitzing, Phys. Rev. Lett. **62**, 1173 (1989); R.R. Gerhardts, D. Weiss, and U. Wulf, Phys. Rev. B **43**, 5192 (1991).

[9] L. Brey, N.F. Johnson, and B.I. Halperin, Phys. Rev. B **40**, 10 647 (1989).

[10] D. Pfannkuche and R.R. Gerhardts, Phys. Rev. B **44**, 13 132 (1991).

[11] P.A. Maksym and T. Chakraborty, Phys. Rev. Lett. **65**, 108 (1990).

[12] D. Pfannkuche, V. Gudmundsson, and P.A. Maksym, Phys. Rev. B **47**, 2244 (1993).

[13] H. Drexler, W. Hansen, J.P. Kotthaus, M. Holland, and S.P. Beaumont, Semicond. Sci. Technol. **7**, 1008 (1992).

[14] U. Wulf and R.R. Gerhardts, in *Physics and Technology of Submicron Structures*, edited by H. Heinrich, G. Bauer, and F. Kuchar, Springer Series in Solid State Sciences Vol. 83 (Springer-Verlag, Berlin, 1988), p. 162.

[15] J.A. Nixon and J.H. Davies, Phys. Rev. B **41**, 7929 (1990).

[16] E.F. Schubert, J. Knecht, and K. Ploog, J. Phys. C **18**, L215 (1985).

[17] G. Weimann and W. Schlapp, in *Two-Dimensional Systems: Physics and New Devices*, edited by G. Bauer, F. Kuchar, and H. Heinrich, Springer Series in Solid State Sciences Vol. 67 (Springer-Verlag, Berlin, 1986), p. 33.

[18] A. Kumar, S.E. Laux, and F. Stern, Phys. Rev. B **42**, 5166 (1990).

[19] B. Meurer, Ph.D. thesis, Universität Stuttgart, 1992.

[20] J. Alsmeier, E. Batke, and J.P. Kotthaus, Phys. Rev. B **41**, 1699 (1990).